Astrophysics and Space Science (2025) 370:7
https://doi.org/10.1007/s10509-025-04396-w

RESEARCH

SDSS-IV MaNGA: the environmental effects on some fundamental properties of early-type galaxies

E. Abdellah[1] · R.M. Samir[2] · Z. Awad[1] · M.Y. Amin[1]

Received: 2 October 2024 / Accepted: 7 January 2025

Abstract
We studied the dependence of selected structural and kinematic properties of early-type galaxies (ETGs) on their environments. The selected sample, extracted from the SDSS-DR17 MaNGA survey, consists of 946 ETGs in clusters (cETGs) and 288 isolated ETGs (iETGs) within a spectroscopic redshift $z \leq 0.15$. We investigated the distribution of these galaxies in the Fundamental Plane (FP), Kormendy Relation (KR), Faber-Jackson Relation (FJR) and the Mass-Size Relation (MSR). We found that massive galaxies, whose stellar masses $M_* > 10^{11} M_\odot$, are predominantly elliptical (> 65%). The analysis of the four scaling relations showed that the effect of the host environment is negligible for massive ($M_* > 10^{11.5} M_\odot$) ETGs, most likely because of their passive evolution through dry mergers and/or stellar aging. On the other hand, low-mass ETGs are influenced by their environment, where iETGs with $M_* < 10^{10} M_\odot$ and velocity dispersion $\sigma_0 \leq 100$ km/sec are 25% more luminous and 11.5% larger than cETGs. Low-mass cETGs may have suffered processes that removed their gas content and hence quenched star formation while low-mass iETGs may have experienced a recent wet merger that triggered star formation and led to their, currently, observed low mass-to-light ratio. However, further spectral analysis is needed to confirm these findings.

Keywords Early-type galaxies · Isolated galaxies · Fundamental plane · Kormendy relation · Faber-Jackson relation · Mass-size relation · Evolution

1 Introduction

Elliptical (E) and lenticular (S0) galaxies form the family of early-type galaxies (*hereafter* ETGs), that have elliptical isophotes (i.e. contours connecting points of equal brightness), and dynamically supported by the random motions (velocity dispersion) of their stars (Ferreras 2019).

✉ E. Abdellah
eabdallah@sci.cu.edu.eg

R.M. Samir
rasha.samir@nriag.sci.eg

Z. Awad
zma@sci.cu.edu.eg

M.Y. Amin
mamin@sci.cu.edu.eg

[1] Astronomy, Space Science and Meteorology Department, Faculty of Science, Cairo University, 12613, Giza, Egypt

[2] National Research Institute of Astronomy and Geophysics (NRIAG), 11421, Helwan, Cairo, Egypt

ETGs are sometimes referred to as quiescent or passive galaxies since they tend to have old, metal-rich stellar populations, with little cold interstellar gas and dust. Hence, they have weak (or absent) stellar formation events, and dominated by a reddish color in the optical band due to their old stellar content (Renzini 2006; Samir et al. 2016; Yoon and Park 2022). This color may indicate the rapid formation of the stellar component within these systems at early epochs, during the formation of the galaxies at $z \geqslant 2$ (Bernardi et al. 1998).

The family of elliptical ETGs possesses a wide range of luminosities; from the very luminous giants ($-24 \leqslant M_B \leqslant -20$) to dwarfs ($-17 \leqslant M_B \leqslant -13$). Consequently, they contain most of the visible mass of the entire Universe (Schechter 1976; Kelvin et al. 2014; Cimatti et al. 2020).

Galaxies are found to follow the morphology-density relation (Dressler 1980) in which galaxies exist in different environments (e.g. clusters, groups, and isolated in the field with no significant neighbors in a given volume (Karachentseva 1973)) with different populations. ETGs are commonly found in clusters, concentrated more toward the cluster core, rather than being isolated (Postman and Geller 1984;

Published online: 27 January 2025

Dressler et al. 1997; Calvi et al. 2012). The dominance of ETGs in denser regions may reflect the environmental role of galactic merging and interactions in their evolution (Samir et al. 2020; Yoon and Park 2022).

In contrast, the smaller fraction of ETGs that are found in isolation allows to probe the evolutionary processes within the galaxy itself, where the environmental physical processes (e.g. tidal interactions, mergers, ram-pressure stripping (Boselli et al. 2022), star-formation quenching (Gu et al. 2021), galactic encounters, etc.) are of less importance. All of these processes are more frequent in denser regions. Therefore, studying the properties of ETGs in high- and low-density regions is crucial in understanding the environmental processes that drive their evolution.

ETGs follow a very tight relationship defined by a thin plane in a three-dimensional parameter space; known as the Fundamental Plane (*hereafter* FP; Djorgovski and Davis 1987; Dressler et al. 1987; Evstigneeva et al. 2002). The FP correlates two surface photometric parameters that are the effective radius, R_e (the radius that contains half of the total light of the galaxy) and $\langle\mu_e\rangle$, which is the mean effective surface brightness within R_e expressed in mag/arcsec^2) and for simplicity it is referred to as the mean surface brightness, with a spectroscopic parameter known as the central velocity dispersion (σ_0). This relationship can generally be expressed as

$$\log(R_e) = \mathrm{a}\ \log(\sigma_0) + \ \mathrm{b}\ \langle\mu_e\rangle + \ \mathrm{c} \tag{1}$$

where the coefficients a and b are the slopes, and c is the intercept, or the zero-point, of the relation. This tight relationship has been interpreted as a consequence of the virial theorem as follows:

$$\log(R_e) = 2\ \log(\sigma_0) + \ 0.4\ \langle\mu_e\rangle\ - \log\left(\frac{M}{L}\right) \tag{2}$$

If ETGs were virialized, perfectly homologous systems and had constant mass-to-light ratios, then the virial theorem would expect a "*virial*" plane of the form

$$\log(R_e) = 2\ \log(\sigma_0) + \ 0.4\ \langle\mu_e\rangle \tag{3}$$

where the values 2 and 0.4 are the predicted values of the coefficients a and b in Eq. (3). However, several studies (e.g. Bernardi et al. 2003b; La Barbera et al. 2010; Samir et al. 2016, 2020; Yoon and Park 2022) showed the observed coefficients are smaller than the predicted ones, with a and b have ranges of (1.0 – 1.6) and (0.30 – 0.35), respectively. This discrepancy between the observed and expected coefficients is known as the '*tilt*' of the FP, and it provides constraints on the formation and evolution of ETGs. The origin of the tilt of the FP can be attributed to some reasons: a consequence of variations in the stellar mass-to-light ratios (Faber et al. 1987; Pahre et al. 1998; Cappellari et al. 2006; de Graaff et al. 2021), the existence of dark matter (Ciotti et al. 1996; de Graaff et al. 2021), different metallicities or ages in the ETGs (Reda et al. 2005; La Barbera et al. 2011; Trevisan et al. 2012; Yoon et al. 2023), and the effect of environments (de Carvalho and Djorgovski 1992; Capelato et al. 1995; Bernardi et al. 2003b; Deng et al. 2008; La Barbera et al. 2010; Samir et al. 2016, 2020; D'Onofrio and Chiosi 2022).

The construction of the FP of ETGs due to mergers was the target of several studies (e.g. Bekki 1998; Aceves and Velázquez 2005; Robertson et al. 2006; Hopkins et al. 2008; Taranu et al. 2015). For example, Robertson et al. (2006) examined the fundamental scaling relations of ETGs, using simulations to deduce the properties of the progenitor galaxies involved into the merger. The results showed that a gas-dissipative merger could contribute to the FP tilt, while dissipationless mergers of disk galaxies should produce remnants that occupy a plane predicted by the virial plane.

An important relation, that correlates the photometric properties of galaxies (R_e and $\langle\mu_e\rangle$) is the Kormendy relation (*hereafter* KR; Kormendy 1977). KR is one of the projections of the fundamental plane, along the ($\log\sigma_o$) axis. It can be written as

$$\langle\mu_e\rangle = \alpha\log(R_e) + \beta \tag{4}$$

where α and β are the KR coefficients. This relation suggests that more luminous ETGs have larger radii and consequently lower surface brightnesses.

Nigoche-Netro et al. (2007a) investigated the effect of gravitational interactions on the behavior of the KR for 82 isolated ETGs, 116 ETGs in the Coma cluster, and a sample of perturbed S0 in dense environments. The results revealed that the KR for all samples have the same behavior, depending on the magnitude range within which the samples were selected, regardless of the environment or the degree of interaction that these ETGs were subjected to. These findings are similar to the results obtained by Reda et al. (2005), Rettura et al. (2010) and Samir et al. (2016).

The Faber-Jackson Relation (*hereafter* FJR) is another projection of the FP that relates the luminosity of the galaxy (L) and its velocity dispersion (σ_0) (Faber and Jackson 1976) via

$$\log(L) = \eta\ \log(\sigma_0)\ +\ \gamma \tag{5}$$

where $\eta \approx 4$. Focardi and Malavasi (2012) studied the effect of the local environment on a sample of 384 nearby elliptical galaxies and found that the scatter of FJR of ellipticals in high-density environments is reduced when compared with those in low-density regions. Samir et al. (2016) studied ETGs in different environments and found that the location of a galaxy along FJR is influenced by its age, with young Es are observed to be brighter and have lower σ_0 compared to the mean relation.

Table 1 Selected MDLM-VAC column names and their descriptions

Column name	The description in MDLM-VAC
T-Type	Morphological T-Type value; T-Type < 0 for early-type galaxies (ETGs) and T-Type > 0 for late-type galaxies (LTGs)
P_{LTG}	Probability of being an LTG; $P_{LTG} > 0.5$ for LTGs and $P_{LTG} < 0.5$ for ETGs
P_{S0}	Probability of being an S0 galaxy; $P_{S0} > 0.5$ for S0s and $P_{S0} < 0.5$ otherwise
Visual_Class	Visual Classification; VC $= 1$ for Es, VC $= 2$ for S0s, VC $= 3$ for Ss and Irr, and VC $= 0$ for unclassified objects
Visual_Flag	Visual classification Flag; VF $= 0$ for certain class and VF $= 1$ for uncertain one

In this study, we aim to present the environmental effects on selected fundamental properties of ETGs by studying their behavior in different scaling relations. The paper is organized as follows. In Sect. 2, we explain the selection of our ETG samples with the quantification of their environments. In Sect. 3, we determine the fundamental properties of our samples. We study different scaling relations of ETG samples and discuss the results in Sect. 4. Finally, we summarize the key results and conclusions in Sect. 5. Throughout this study, we adopt a flat cosmological model with parameters: $\Omega_m = 0.3$, $\Omega_\Lambda = 0.7$, and Hubble's constant $H_0 = 70$ km s^{-1} Mpc^{-1}.

2 Galaxy sample and selection criteria

In this section we describe the strategy of selecting our sample of ETGs and the criteria by which we identified their host environment. Galaxy samples were extracted from the seventeenth data release (*hereafter;* DR17) of the final release of the fourth phase of the Sloan Digital Sky Survey (SDSS-IV; Abdurro'uf et al. 2022). DR17 includes the complete release of Mapping Nearby Galaxies at Apache Point Observatory (MaNGA) survey (described elsewhere; Bundy et al. 2015). The strength of SDSS-IV MaNGA survey comes from the unprecedented large sample of nearly 10,000 galaxies, and from its ability to probe a wide range of environments where galaxies reside. MaNGA uses Integral Field Units (IFUs) to measure multiple spectra across the 10,000 nearby galaxies.

We created our samples from the MaNGA survey, in the r-band, by the following strategy: we, firstly, used the *MaNGA Deep Learning Morphology DR17 Value-Added Catalog* (MDLM-VAC; see Domínguez Sánchez et al. 2022) to select galaxies that are morphologically classified as ellipticals (Es) and lenticulars (S0s). Secondly, we identified the environment of the selected ETGs (isolated or in clusters) with the *Galaxy Environment for MaNGA Value-Added Catalog* (GEMA-VAC; Argudo-Fernandez et al. 2021). Finally, the photometric and spectroscopic observable parameters of our samples and their errors were extracted with the help of Catalog Archive Server Jobs System (CasJobs), which is available online through the SDSS website.[1] In the following subsections we are going to describe the details of our selection strategy.

2.1 Morphological classification

The morphological classification of the MaNGA galaxies, appeared in MDLM-VAC, is performed with the aid of convolutional neural networks (Domínguez Sánchez et al. 2022). The catalog contains 10,293 classified galaxies, however some of them have duplicated spectroscopic observations. The individual spectroscopically observed MaNGA galaxies are 10,127 (see Domínguez Sánchez et al. 2022, Table 4). We combined the information in Table 1 for selecting MaNGA-ETGs as follows:

1. **For Es**: (T-Type < 0) and ($P_{LTG} < 0.5$) and ($P_{S0} < 0.5$) and (VC $= 1$) and (VF $= 0$).
2. **For S0s**: (T-Type < 0) and ($P_{LTG} < 0.5$) and ($P_{S0} > 0.5$) and (VC $= 2$) and (VF $= 0$).

Applying these criteria and filtering the sample for duplication, we obtained 3310 galaxies; 2430 of which are Es and 880 are S0s.

2.2 Identification of the host environments

We identified the environments where the MaNGA-ETGs are located using GEMA-VAC in DR17, which contains quantifications of the environments for MaNGA galaxies. GEMA-VAC has 15 Header Data Units (HDUs) to characterize the environments of 10,087 galaxies. A general description of the contents of the catalog can be found in SDSS Data Model website[2] (Argudo-Fernandez et al. 2021) as well as through the Marvin[3] interface (Cherinka et al. 2019).

2.2.1 Isolated ETGs

Based on the techniques described by Argudo-Fernández et al. (2015), a galaxy is considered isolated (with no neighbors) within the line-of-sight if the velocity difference, Δv,

[1] CasJobs: https://skyserver.sdss.org/CasJobs/.

[2] GEMA: https://data.sdss.org/datamodel/files/MANGA_GEMA/.

[3] Marvin: https://dr17.sdss.org/marvin/.

is $\leqslant$ 500 km s^{-1}, in a field radius $d_{\rm NN} \geqslant 1$ Mpc, where $d_{\rm NN}$ is the projected distance to the first nearest neighbor of this galaxy. The HDU7, in GEMA-VAC, quantifies the Large Scale Structure (LSS) environment up to 5 Mpc projected distance for all observed redshifts in MaNGA survey.

According to Argudo-Fernández et al. (2015), the selection criterion for isolated galaxies in this study is 1 Mpc $\leqslant d_{\rm NN} \leqslant 5$ Mpc. The number of selected isolated MaNGA galaxies is 1449. We cross-matched the morphologically selected 3310 MaNGA-ETGs with the 1449 isolated MaNGA galaxies and obtained a sample of 382 isolated ETGs (*hereafter* iETGs).

2.2.2 ETGs in clusters

In HDU15, the LSS environments where galaxies reside can be characterized by the eigenvalues of the tidal tensor along the major, intermediate and minor axes at the galaxy's position (Hahn et al. 2007; Wang et al. 2016). These eigenvalues are labeled t_1, t_2 and t_3. Galaxies in LSS environments are characterized as follows:

1. **Cluster:** $t_1 > 0, t_2 > 0, t_3 > 0$.
2. **Filament:** $t_1 > 0, t_2 > 0, t_3 < 0$.
3. **Sheet:** $t_1 > 0, t_2 < 0, t_3 < 0$.
4. **Void:** $t_1 < 0, t_2 < 0, t_3 < 0$.

According to this rule, our sample contains 2872 galaxies in clusters. This number was reduced to 1230 after cross-matching with the morphologically selected sample. These galaxies will be referred to as cETGs in the rest of this paper.

In order to ensure that no duplicated galaxies were in both samples, we cross-matched both samples together and excluded 60 duplicated galaxies. This resulted in a whole sample of 322 iETGs and 1170 cETGs. The equatorial coordinates (RA and DEC) of these galaxies were imported in CasJobs to extract their photometric and spectroscopic parameters required for this study.

2.3 ETGs parameters extraction using CasJobs

The extracted photometric and spectroscopic parameters with their descriptions are shown in Table 2. We set the search radius between the position of our sample galaxies and the SDSS primary object to be 2″, and obtained the parameters of 310 iETGs and 1130 cETGs. After excluding the objects that are classified as Quasi-stellar Objects (QSOs; 4 from iETGs and 1 from cETGs), we got 306 iETGs and 1129 cETGs.

Moreover, we considered only galaxies having values of velocity dispersion and/or σ_0 between 75 km s^{-1} and 350 km s^{-1} (see Sect. 3.1.4). The reason for choosing this range is that velocity dispersion values $<$ 70 km s^{-1} may come from significant spectral uncertainties (Hou and Wang 2015) while those $>$ 350 km s^{-1} may result from objects observed in superposition, which affects the strength of the spectral absorption lines (Bernardi et al. 2006, 2008).

We also calculated the relative errors for the extracted parameters of both samples to ensure that they do not exceed 0.5. Thus, the final number of iETGs and cETGs are 288 and 946, respectively, with spectroscopic redshift, velocity dispersion and σ_0 ranges listed in Table 3.

Finally, to ensure that the galaxies in our samples are bulge-dominated, we checked the weight values (from 0 to 1) of the de Vaucouleurs fit component in the combined model of de Vaucouleurs and exponential disk fit in the r-band (the $fracDev\_r$ in SDSS tables). We found that about 97% of cETGs and about 95% of iETGs have $fracDev\_r \geqslant 0.7$. Thus, our final whole sample is bulge-dominated, whose surface brightness profiles are well described by the de Vaucouleurs model (de Vaucouleurs 1948).

3 Methodology

In order to study the environmental effects on the evolution of the galaxies, we need to study the correlations between the galactic fundamental parameters. These correlations are known as the scaling relations. We calculated these fundamental parameters from the observable parameters extracted by using SDSS CasJobs tool. The observable parameters we used were reduced and analyzed previously by Westfall et al. (2019). It is important to mention that all of the following calculations and measurements were performed using TOPCAT (Tool for OPerations on Catalogs And Tables) software (Taylor 2005), as well as some Python Packages.

3.1 Determining fundamental parameters

3.1.1 The effective radius

To calculate the R_e, we should first calculate the effective angular radius, r_0 (Eq. (6)) following Samir et al. (2020)

$$r_0 = r_{\rm dev} \sqrt{\frac{b}{a}} \tag{6}$$

where $r_{\rm dev}$ is the de Vaucouleurs angular radius in arcsec and (b/a) is the de Vaucouleurs axial ratio. We then convert r_0 in arcsec to the physical effective radius, R_e, in kpc (Eq. (7)).

$$R_e = r_0 \ D_A(z) \tag{7}$$

where $D_A(z)$ is the angular distance at redshift, (z), in kpc/″, which is calculated using the cosmological calculator (Wright 2006) which is available at NASA/IPAC Extragalactic Database (NED).[4]

[4]NED: https://astro.ucla.edu/~wright/CosmoCalc.html.

Table 2 Extracted parameters, their symbols, descriptions and units, and the table names from which they were obtained from the CasJobs tool in SDSS

Parameter	Symbol	Parameter description	Table name	Unit
deVRad_r[a]	r_{deV}	de Vaucouleurs radius which is defined as the half-light radius	*Galaxy*	arcsec
deVRadErr_r	Δr_{deV}	Error in de Vaucouleurs radius	*Galaxy*	arcsec
deVAB_r	b/a	de Vaucouleurs axis ratio	*Galaxy*	–
deVABErr_r	$\Delta b/a$	Error in de Vaucouleurs axis ratio	*Galaxy*	–
extinction_r[b]	A_r	extinction in the r-band	*Galaxy*	mag
cModelMag_r[c]	$m_{c,r}$	Composite model magnitude in the r-band, which describes the better fitting of the combined exponential and de Vaucouleurs models together	*Galaxy*	mag
cModelMagErr_r	$\Delta m_{c,r}$	Error in composite model magnitude in the r-band	*Galaxy*	mag
fracDev_r		Weight of deV component in (deV+Exp) model in the r-band	*Galaxy*	
kcorrR[d]	$k(z)_r$	The k-correction in r-band for $z = 0$	*Photoz*	–
zs[e]	z	Spectroscopic redshift	*SpecObj*	–
zsErr	Δz	Error in spectroscopic redshift	*SpecObj*	–
velDisp	σ	The velocity dispersion	*SpecObj*	km s^{-1}
velDispErr	$\Delta\sigma$	Error in velocity dispersion	*SpecObj*	km s^{-1}
class		Spectroscopic class of the object; QSO or Star or Galaxy	*SpecObj*	–
logMass[f]	$\log M_*$	Best-fit of the galaxy stellar mass	*stellarMassPassivePort*	$M_\odot$

[a]Fitting models for de Vaucouleurs radius and axis ratio are described here (https://www.sdss4.org/dr17/algorithms/magnitudes/#ModelMagnitudes:devMag,expMag,modelMag)

[b]Details of obtaining the extinction parameter are elsewhere; see (https://www.sdss4.org/dr17/algorithms/magnitudes/#ExtinctionCorrection)

[c]The methodology of obtaining the composite model magnitude and fracDeV is described in the SDSS website at (https://www.sdss4.org/dr17/algorithms/magnitudes/#CompositeModelMagnitudes:cModelMag)

[d]Beck et al. (2016) and (https://www.sdss4.org/dr17/algorithms/photo-z/#PhotozsupdatedinDR12,unchangedinDR13andlaterdatareleases)

[e]Details on obtaining the three spectroscopic parameters are described in Bolton et al. (2012) and (https://www.sdss4.org/dr17/algorithms/redshifts/#VelocityDispersions)

[f]Stellar masses are estimated using models by Maraston et al. (2009) that adopted the Kroupa IMF (Kroupa 2001) for passive stellar evolution. The errors in logMass in the plots were obtained by extracting the parameters minLogMass and maxLogMass.

Table 3 Spectroscopic redshift, velocity and central velocity dispersion ranges for our final samples

Sample	Redshift	Velocity dispersion (km s^{-1})	Central velocity dispersion (km s^{-1})
iETGs	$0.018 < z < 0.15$	$77 < \sigma < 321$	$84 < \sigma_0 < 340$
cETGs	$0.015 < z < 0.12$	$75 < \sigma < 343$	$77 < \sigma_0 < 348$

3.1.2 The mean surface brightness

The mean surface brightness is the surface brightness of the galaxy enclosed within R_e and expressed in terms of magnitudes as $\langle \mu_e \rangle$. We calculated the $\langle \mu_e \rangle$ in mag/arcsec^2 via Eq. (8) following Hou and Wang (2015) and Samir et al. (2020).

$$\langle \mu_e \rangle = m_{c,r} - A_r + 2.5\log(2\pi r_0^2) - k(z)_r - 10\log(1+z) + Q\,z \tag{8}$$

where $m_{c,r}$ is the composite model magnitude, A_r is the extinction, $k(z)_r$ is the k-correction. All of these quantities are measured in the r-band. z is the spectroscopic redshift and Q is the correction factor in luminosity for the evolution of the galaxy. According to Bernardi et al. (2003), the Q values are set to be 1.15, 0.85, 0.75 and 0.60 for *griz* bands, respectively. We set the value to $Q = 0.85$ which corresponds to the r-band.

3.1.3 The absolute magnitude

It is possible to express the luminosity of a galaxy, L, in terms of its absolute magnitude, M, in the r-band by Eq. (9), following Samir et al. (2020)

$$M_r = m_{c,r} - 5\log\left(\frac{D_L}{10pc}\right) - A_r - k(z)_r + Q\,z \tag{9}$$

where D_L is the luminosity distance which is calculated with the spectroscopic redshift of the galaxy, using the NED cosmological calculator.

3.1.4 The central velocity dispersion

The angular radius of the fixed fiber aperture of the SDSS spectrograph is $1.5''$. Thus, the observed velocity dispersion, σ, of any galaxy with a larger angular radius than that of the spectrograph will reflect the motion of the innermost stars compared to another galaxy with a smaller angular radius. It is therefore necessary to apply an aperture correction for the observed velocity dispersion to obtain the *"central"* velocity dispersion, σ_0. In this case, the comparison among different galaxies with different sizes is meaningful (Jorgensen et al. 1995; Wegner et al. 1999). The applied correction for the values of σ_0 is adopted from Hou and Wang (2015)

$$\sigma_0 = \sigma\left(\frac{r_{\rm fiber}}{r_0/8}\right)^{0.04} \tag{10}$$

where $r_{\rm fiber}$ is the angular radius of the fiber ($1.5''$ in our study) and r_0 is the effective angular radius, previously calculated using Eq. (6).

3.2 Least trimmed squares technique

The Least Trimmed Squares (LTS) fitting technique is based on the Chi-squared (χ^2) minimization after excluding (i.e. trimming) the outliers, from inside out, and therefore, LTS reduces the scattering around the best-fit plane (for three dimensional, 3D, data sets) or line (for two dimensional, 2D). In this work, a data point is considered an outlier if it deviates more than three times the standard deviation (σ) of the data.

Applying the LTS on a 3D set of data (x_i, y_i, z_i) with symmetric errors (Δx_i, Δy_i, Δz_i) generates a best-fit plane on the form $z = ax + by + c$. In this case, the scattering is reduced along the z-direction (ε_z). Similarly, for a 2D set of points (x_i, y_i) with symmetric errors (Δx_i, Δy_i), the best-fit line takes the form $y = \alpha x + \beta$.

We investigated the scaling relations of our samples using the python package LTSFIT[5] (Cappellari et al. 2013; Yoon and Park 2022).

4 Results and discussion

In this section we present and discuss the results of the four scaling relations for c- and i-ETGs and the impact of the host environment on their properties. The effect of the environment is measured by defining the comparison parameter, $\sigma_{\rm comp}$, which is calculated considering the cluster environment as the reference environment. The parameter $\sigma_{\rm comp}$ for any fitting coefficient, for instance a, can be expressed as

$$\sigma_{\rm comp} = (a_c - a_i)/\Delta a_c$$

[5]LTSFIT python package: https://www-astro.physics.ox.ac.uk/~cappellari/software.

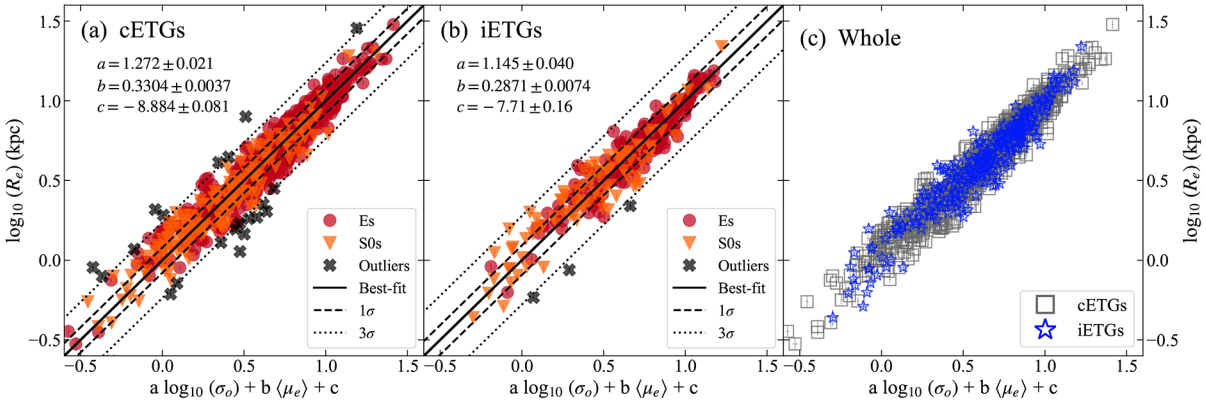

Fig. 1 Fundamental Plane for ETGs (a) in clusters (cETGs) and (b) isolated (iETGs). In both panels, red circles are ellipticals (Es), orange triangles are lenticulars (S0s) while black crosses are the trimmed outliers. Solid lines represent the best-fit lines whereas dashed and dotted lines are the 1σ and 3σ deviations, respectively. The coefficients of the FP (a, b, c) are listed for each sample. Panel (c) shows the FP of the whole ETG sample in this work (see key). All data points are plotted with their error bars

Table 4 A summary of coefficients of the FP obtained for both ETG samples using the Least-trimmed squares (LTS) fitting technique. Column (1) is the galaxy sample. Columns (2-3) are the σ_0- and $\langle\mu_e\rangle$- slopes while column (4) is the zero-point. Columns (5-6) show the intrinsic scatter and the standard deviation

Sample	Fitting coefficients				
	$(a \pm \Delta a)$	$(b \pm \Delta b)$	$(c \pm \Delta c)$	$(\varepsilon \pm \Delta\varepsilon)$	1σ
cETGs	1.272 ± 0.021	0.3304 ± 0.0037	-8.884 ± 0.081	0.0763 ± 0.0020	0.079
iETGs	1.145 ± 0.040	0.2871 ± 0.0074	-7.71 ± 0.16	0.0895 ± 0.0043	0.093

where Δa_c is the uncertainty in the obtained coefficient and the subscripts (c and i) stand for c- and i-ETGs, respectively. The effect of the environment is determined through the condition

$$\text{if} \quad \sigma_{\text{comp}} \begin{cases} > 3, & \text{has effect} \\ \leq 3, & \text{no effect} \end{cases}$$

4.1 The fundamental plane

Figure 1 shows the fundamental plane for cETGs, panel (a), and iETGs, panel (b). For both samples, red circles represent elliptical galaxies, orange triangles are the lenticulars. Solid lines represent the best linear fitting while dashed and dotted lines are the 1σ and 3σ standard deviations for both samples, respectively. Galaxies denoted by thick black crosses were excluded and considered outliers (i.e. have values of $R_e, \langle\mu_e\rangle, \sigma_0$ that deviate $> 3\sigma$). Our sample contains 22 cETG and 3 iETG outliers. Also, the coefficients of FPs of both samples were inserted in each panel, where we plot the x-axis as $(a \log\sigma_0 + b \langle\mu_e\rangle + c)$. Moreover, we display the distributions along the FP for both samples together in panel (c), where cETGs and iETGs are represented by grey squares and blue stars, respectively. The slopes, zero-points, intrinsic scatter and the 1σ deviation around the linear fitting of both samples are reported in Table 4.

The distribution of both samples shows different coefficients. From the fitting, the velocity dispersion slope, a, the slope of $\langle\mu_e\rangle$, b, and the zero-point, c, for cETGs are 1.272 ± 0.021, 0.3304 ± 0.0037 and -8.884 ± 0.081, respectively. On the other hand, these values are 1.145 ± 0.040, 0.2871 ± 0.0074 and -7.71 ± 0.16 for iETGs, respectively. It is clear that a, b and c for iETGs are within $7\sigma_{\text{comp}}$, $12\sigma_{\text{comp}}$ and $15\sigma_{\text{comp}}$ of those for cETGs, respectively. Finally, the intrinsic scatter ε around the FP of cETGs is 0.0763 while it is 0.0895 for iETGs, as cETGs are obviously less scattered around the FP than iETGs.

According to the virial theorem (see Eqs. (1) and (2)), the value of the zero-point, c, provides an estimate for the mass-to-light (M/L) ratios of galaxies. cETGs have a smaller zero-point value than iETGs, which may indicate that cETGs have older stellar populations than iETGs. As a result, cETGs would have larger M/L ratios than iETGs. In addition, the relatively larger coefficient a for cETGs indicates that cETGs have higher values of σ_0 than iETGs. Although, we excluded σ_0s higher than 350 km s^{-1}, the large value of a for cETGs implies that most of these galaxies have higher σ_0, compared to iETGs. Moreover, the larger $\langle\mu_e\rangle$ coefficient, b, for cETGs indicates that cETGs have higher $\langle\mu_e\rangle$ (i.e. lower surface brightnesses, I_e) than iETGs. The reason for that can be attributed to the large fraction of

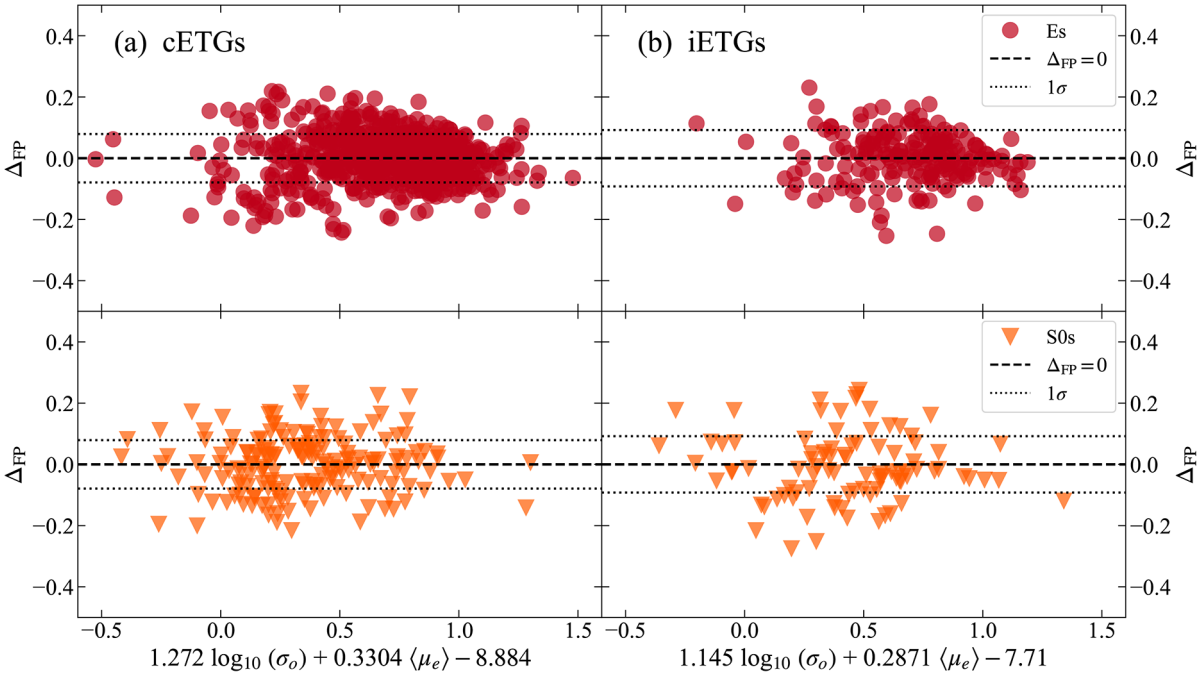

Fig. 2 Residuals around the FP for (a) cETGs and (b) iETGs where the upper panels show ellipticals and the lower panels display the lenticulars (see key). Dashed line indicates $\Delta_{FP}=0$ whereas the dotted line is the 1σ deviation of the data points

less-luminous cETGs that have relatively larger sizes than that of iETGs.

It is clear from panels (a) and (b) in Fig. 1 that in both environments, Es are more concentrated toward larger sizes (R_e), higher σ_0 values and higher values of $\langle\mu_e\rangle$, whereas the majority of S0s are distributed along the FP, with a small fraction lying in the regions with larger R_e. Also, Es show less scatter around the linear relation when compared with S0s in both environments.

In Fig. 2, we analyze the residuals of both samples around their FPs, Δ_{FP}, to examine their deviations around the FP via

$$\Delta_{FP}=\log(R_e)\ -\ a\ \log(\sigma_0)\ -\ b\ \langle\mu_e\rangle\ -\ c \qquad (11)$$

The coefficients in Eq. (11) are set for cETGs and iETGs, as obtained from the LTS fitting. In order to obtain a reasonable comparison between both samples, we separated Es from S0s in the samples and plotted each morphological sub-sample with respect to $\Delta_{FP}=0$, which represents the zero-error around the FP. It is clear from the upper panels in Fig. 2 that Es are less scattered around the FP, with a large fraction concentrated toward larger R_e, regardless of their host environment. On the other hand, the distribution of S0 residuals in both environments (lower panels) shows that they are more scattered than Es, especially isolated S0s, with a small number having large R_e. This can be explained as a consequence of age and/or metallicity variations in larger ETGs.

We compare the derived coefficients of the FP of our cETG sample with La Barbera et al. (2010) who studied a sample of 39,993 ETGs with redshift $z<0.1$. Their σ_0 coefficient ($a=1.39$) is larger than ours by about 6σ while their $\langle\mu_e\rangle$ coefficient ($b=0.314$) is smaller by about 4σ. However, their zero-point coefficient ($c=-8.867$) is within the same range of our value. The FP coefficients of the iETGs are compared with 550 isolated ellipticals (*hereafter*; IEs) with redshift $z\leq 0.08$ (Samir et al. 2020). Their a value ($a=1.43$) is larger by about 7σ than ours whereas the value of b of their sample ($b=0.29$) is within the same value of ours. The value of $c=-8.48$ is smaller than ours by about 5σ.

The general trend of the FP of cETGs and iETGs may indicate that the environment has an influence on the observed properties of these nearby ETGs. iETGs may have suffered a recent wet (gaseous) merger, resulting in their small M/L ratios, i.e. younger stellar population (Reda et al. 2005; Cappellari et al. 2013; Samir et al. 2016) while cETGs may have passively evolved or undergone a few dry minor mergers, causing an increase in the sizes of a large fraction of them. Thus, gaseous merger route may be responsible for the obtained FP coefficients of iETGs while passive evolution and/or dry mergers may explain cETGs derived coefficients (Bernardi et al. 2003b).

Bernardi et al. (2003b) found that ETGs reside in dense regions are slightly less luminous (fainter) and possess higher σ_0 than ETGs in less dense regions. This finding is inline with the present work as we find that about 49% of our cETGs and about 38% of iETGs have $\log\sigma_0\geq 2.35$. Bernardi et al. (2003b) concluded that the observed evo-

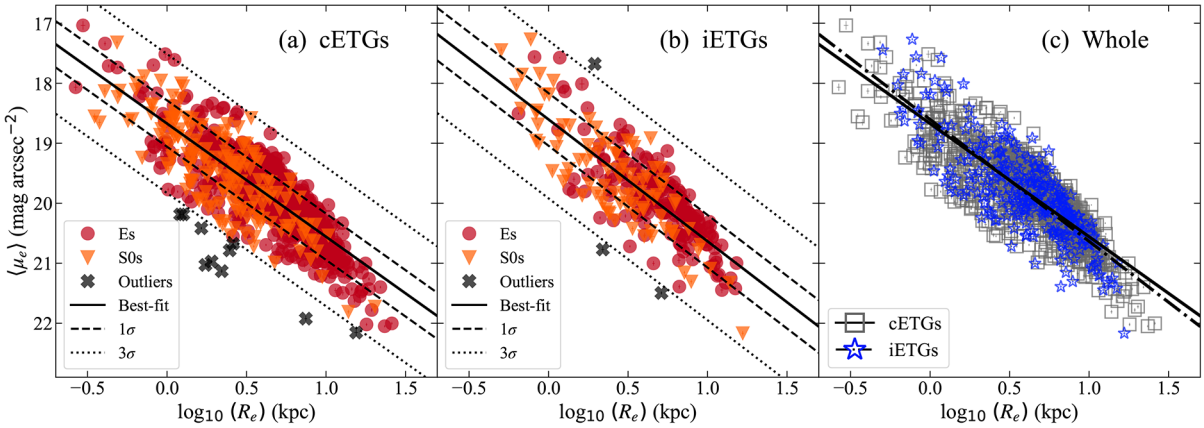

Fig. 3 Kormendy relation for (a) cETGs, (b) iETGs and (c) the whole sample (see key)

lution in the galaxy properties was consistent for ETGs in dense regions that formed the majority of their stars about 9 Gyrs ago and have been passively evolving since then, which is in agreement with the present work. However, Reda et al. (2005) found, for a sample of 23 isolated ETGs, that those ETGs follow the same tilt and scatter of the FP of the Coma-cluster galaxies, except for a few deviant galaxies that have smaller M/L ratios (i.e. have younger stellar population) as expected from a recent gaseous merger.

D'Onofrio et al. (2008) analyzed the FP of ETGs in 59 nearby clusters ($0.04 < z < 0.07$) and found that there is a strong correlation between the FP coefficients and the local galaxy density (ρ). Their results showed that as the galaxy density increases, the FP coefficients a and b increases while c decreases, which is consistent with our findings. Hyde and Bernardi (2009) found that the scatter around the FP is larger for smaller sizes and less-massive galaxies. Bernardi et al. (2020) found that the thickness of the FP depends strongly on the morphology of the galaxies included in the sample. For slow-rotating Es only, the observed scatter is reduced to $\sim 16\%$ while for fast-rotating Es and S0s, the observed scatter increases to $\sim 25\%$. These results are in agreement with ours.

La Barbera et al. (2010) attributed the decrease of the slope (a) with local galaxy density, to environmental effects such as tidal stripping. This decrease in the slope (a) contradicts with our results. This discrepancy may be due to the small cut-off of σ_0, (< 75 km/sec). However, La Barbera et al. (2010) found that the coefficient, b, is larger for galaxies in massive clusters and in galaxy groups than for field galaxies. Also, the authors concluded that galaxies in low-density environments have lower mass-to-light ratios than those in high-density regions, indicating younger stellar population, which is consistent with the results of this work.

Moreover, Forbes et al. (1998), Samir et al. (2016) and Yoon and Park (2020) found that the scattering in the FP is smaller for old ETGs while young ETGs exhibited larger scattering in the FP, which indicates that the scenario of a recent gaseous major merger can be responsible for the large scatter of younger ETGs.

Furthermore, Samir et al. (2020) found that the brightest cluster galaxies (*hereafter*; BCGs), having higher σ_0 than the IEs, lie on a FP slightly different from that of IEs, with BCGs showing larger coefficients a and b compared to IEs. They suggested a diversity in the structural and dynamical properties of BCGs and IEs, leading to their different FPs. They also found smaller scatter around FP of BCGs than of IEs. Similar results were obtained by Yoon and Park (2022) who divided their sample into bins of specific σ_0 intervals and found a smaller scatter for higher values of σ_0. Thus, these results are in agreement with ours.

4.2 Kormendy relation

Figure 3 represents the Kormendy relation (KR) which relates R_e and $\langle\mu_e\rangle$ for cETGs (panel a) and iETGs (panel b). A holistic view of the KR for both samples is given in panel (c) of the same figure. The excluded outliers are 10 from cETGs and 3 from iETGs. Table 5 shows the values of the best-fitting coefficients (from Eq. (4)), 1σ deviation and the intrinsic scatter around the relation.

We found a little statistically-detected dependence of the galaxy distribution of both samples on their host environment which is clearer from their best-fitting coefficients (Table 5). In general, the slope (α) for iETGs (2.030 ± 0.084) is within $4\sigma_{\rm comp}$ of that for cETGs (1.886 ± 0.039). The zero-point (β) for iETGs (18.604 ± 0.057) is within $3\sigma_{\rm comp}$ of that for cETGs (18.672 ± 0.027). Comparing the intrinsic scatter (ε) for both samples, we find that the intrinsic scatter around cETGs is slightly smaller than that of iETGs.

In Fig. 3, in both environments, most of the Es (circles) are concentrated toward larger R_e and higher $\langle\mu_e\rangle$ while the distribution of the majority of S0s (triangles), with a small fraction of Es, is scattered over the whole range of sizes

Table 5 KR coefficients for our ETG samples obtained using LTS fitting technique. Slopes (column 2), zero-points (column 3), intrinsic scatters (column 4) and 1σ deviation (column 5) are displayed for both ETG samples

Sample	Fitting coefficients			
	$(\alpha \pm \Delta\alpha)$	$(\beta \pm \Delta\beta)$	$(\varepsilon \pm \Delta\varepsilon)$	1σ
cETGs	1.886 ± 0.039	18.672 ± 0.027	0.3849 ± 0.0093	0.39
iETGs	2.030 ± 0.084	18.604 ± 0.057	0.437 ± 0.020	0.44

and brightnesses. It is clear, from panel (c), that both samples have nearly similar behavior where large galaxies tend to be less scattered around the best-fit lines than smaller ones. Also, for any R_e value, we found values of $\langle\mu_e\rangle$ to be nearly identical for both samples. For example, galaxies with $\log(R_e) = 1$ have $\langle\mu_e\rangle$ value of about 20.6 mag/arcsec^2 (see Table 5).

The slope (α) of KR for our cETGs is smaller by about 43σ than that for ETGs studied by La Barbera et al. (2010) where they obtained $\alpha = 3.55$. On the other hand, for our iETG sample, it is smaller by about 22σ than that for IEs studied by Samir et al. (2020) for which $\alpha = 3.87$. However, the zero-points (β) for our c- and i-ETGs are larger by about 19σ and 13σ than that of La Barbera et al. (2010) and Samir et al. (2020) which, for both studies, are $\beta = 18.16$ and 17.87, respectively. This differences may be attributed to different fitting procedures.

The obtained results of KR for both environments are consistent with the scenario of environmental dependence during their formation. Assuming that larger and massive ETGs have experienced dry mergers, this can effectively increase the sizes and stellar masses of the merging remnants leaving their luminosities and velocity dispersions similar to their progenitors. This scenario leads to the currently observed large and massive remnants with lower surface brightnesses (e.g. higher $\langle\mu_e\rangle$).

Moreover, if we assume for smaller ($\log(R_e) < 0.02$) and less-massive ($\log(M_*/M_\odot)) < 10$) cETGs, tidal and ram-pressure stripping could effectively remove their gas content, the current observed properties would be smaller and less-luminous galaxies due to the quenching of star formation. On contrary, assuming wet mergers for smaller and less-massive iETGs, this would lead to the formation of new stars, and hence a more-luminous (i.e. lower $\langle\mu_e\rangle$) remnant.

Hamabe and Kormendy (1987) re-derived the KRs for elliptical galaxies and bulges on the form $\mu_{e,V} = 2.94 \log R_e + 19.48$, to which the coefficients of our samples are shallower. Nigoche-Netro et al. (2007b) compared a sample of isolated ETGs with a sample of ETGs in the Coma Cluster and perturbed S0 galaxies. They found similar KRs for isolated ETGs, galaxies in high-density environments and galaxies in interaction. These findings are inline with the outcomes of Reda et al. (2005), Rettura et al. (2010) and Samir et al. (2016) where changing the host environment does not effectively affect the KR, in agreement with the current study.

In addition, Rettura et al. (2010) found a fraction of ETGs in the field have longer timescales to assemble their mass, compared to their peers in clusters. Also, their results showed that the formation epoch of ETGs depends on their mass while the environment regulates the timescales of their star formation histories. This finding is in agreement with ours. Moreover, Samir et al. (2020) showed a KR for BCGs, with shallower slope than IEs, that is similar to that of the bright family which confirms their formation out of highly evolved objects that experienced merging events, inline with our results.

4.3 Faber-Jackson relation

The Faber-Jackson relation (FJR) relates the σ_0 and the luminosity in the r-band (L_r). Figure 4 represents this relation for our samples as indicated in the figure key. 15 cETG and 3 iETG outliers were excluded from the samples. Table 6 lists the slopes, zero-points, intrinsic scatter, and the 1σ deviation for both samples as obtained for this relation (Eq. (5)).

The slope (η) of iETGs (2.451 ± 0.093) is within $6\sigma_{\rm comp}$ of that for cETGs (2.752 ± 0.058). The zero-point (γ) of iETGs (5.01 ± 0.21) is within $6\sigma_{\rm comp}$ of that for cETGs (4.28 ± 0.13). Although the slopes of both samples deviate from the original relation ($\eta \approx 4$), this should reflect something about the evolution of the properties of our samples. Comparing the intrinsic scatter for both samples, we found that both samples have similar scattering around the fitting line of the relation. The slope (η) of FJR for our cETGs is much smaller by about 42σ than that obtained by La Barbera et al. (2010) which equals 5.208, whereas for iETGs it is smaller by about 2σ than the IEs obtained by Samir et al. (2020) for which $\eta = 2.63$.

From Fig. 4 one can notice that most of the Es (circles) have higher L_r and σ_0 values, but all of the S0s (triangles) show highly scattered distribution in both environments. This behavior can be is explained in terms of the order of stellar motion in each galaxy type. S0 galaxies generally have moderately ordered stellar orbits, thus called fast rotators, while stars in more massive and luminous Es have random motions and hence Es are known as slow rotators. Therefore, slow rotators are expected to have higher σ_0 regardless of their environment compared to fast rotators and less luminous Es (see panel (c) in Fig. 4).

For higher σ_0 values, ETGs in both samples have nearly the same luminosity. For example, at $\sigma_0 = 300$ km/sec, the

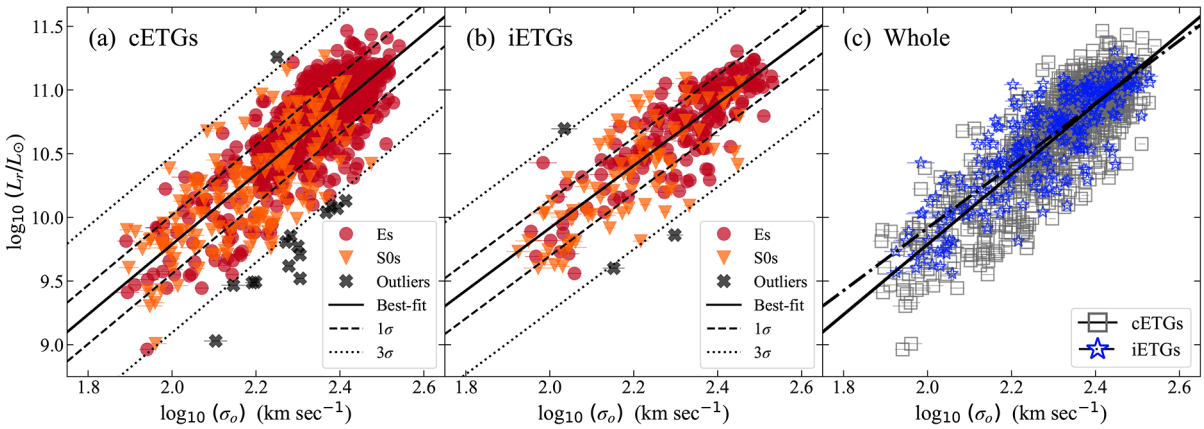

Fig. 4 Faber-Jackson relation for (a) cETGs and (b) iETGs while (c) shows FJR for the whole sample (see key)

Table 6 FJR coefficients for our ETG samples obtained using LTS fitting technique. Slopes (column 2), zero-points (column 3), intrinsic scatters (column 4) and 1σ deviation (column 5) are displayed for both ETG samples

Sample	Fitting coefficients			
	$(\eta \pm \Delta\eta)$	$(\gamma \pm \Delta\gamma)$	$(\varepsilon \pm \Delta\varepsilon)$	1σ
cETGs	2.752 ± 0.058	4.28 ± 0.13	0.2273 ± 0.0056	0.23
iETGs	2.451 ± 0.093	5.01 ± 0.21	0.2147 ± 0.0100	0.22

ratio of the luminosity of cETGs to iETGs is almost unity. This indicates that luminous ETGs have more randomized stellar motions, regardless of their environments. However, for smaller values of σ_0, we find that iETGs are more luminous than cETGs with the same σ_0. For example, if we take $\sigma_0 = 100$ km/sec, we find that cETGs are $\sim 25\%$ less luminous than iETGs and hence less massive cETGs are less luminous than their counterparts in the field. The observed trend is influenced by the environment which may have an impact during the early phases of ETGs formation. Slow-rotating (higher σ_0) cETGs and iETGs have very similar luminosity, which agrees with the scenario of rapid formation of massive ETGs at early epochs and their passive evolution. Therefore, these massive, luminous and old ETGs in both environments have similar kinematic and structural properties (Bernardi et al. 2003b). On the other hand, mechanisms such as a ram-pressure stripping and tidal interactions would suppress any star formation in fast-rotating cETGs and cause them to appear fainter. In addition, fast-rotating iETGs show an agreement with the scenario of wet mergers, causing star formation and thus the relatively observed luminous merger remnants.

Emsellem et al. (2007) found that fast rotators tend to be relatively less-luminous galaxies while slow rotators appear brighter and more massive galaxies. They suggested that slow rotators are the extreme evolutionary end-point reached deep in gravitational potential wells where dissipationless (dry) mergers played a major role in the evolution. This finding is inline with our results. Nigoche-Netro et al. (2011) showed that the intrinsic dispersion depends on luminosity, mass, and redshift, with brighter and more massive galaxies have smaller intrinsic dispersion compared to fainter and less massive ones, that is consistent with our findings. The authors concluded that the intrinsic dispersion in the FJR may depend on the formation and evolution history of galaxies. Moreover, Focardi and Malavasi (2012) found that the scatter in the FJR was significantly reduced when Es in high-density environments are compared to those in low-density environments, which is in agreement with our result.

Samir et al. (2016) found that young ETGs are observed to be brighter and/or have lower σ_0 compared to the mean relation. Samir et al. (2020) showed that BCGs follow a FJR of the form $L \propto \sigma_0^{6.25}$ while IEs have a different FJR of the form $L \propto \sigma_0^{2.63}$. The slope of their IEs sample is similar to our iETGs, but the FJR of their BCGs shows a steeper slope because of the nature of this ETG class. Domínguez Sánchez et al. (2020) found that at a fixed σ_0, more luminous S0s and fast-rotating Es are younger than slow-rotating Es, in agreement with our results. Yoon and Park (2022) found that for a fixed σ_0, luminous and massive ETGs are observed to have higher μ_e and concluded that the dry merger route may be responsible for the observed properties of ETGs which is inline with ours.

4.4 Mass-size relation

One of the most important relations that has been studied to investigate how galaxies assemble their masses and grow in size is the relation between the size (expressed by R_e)

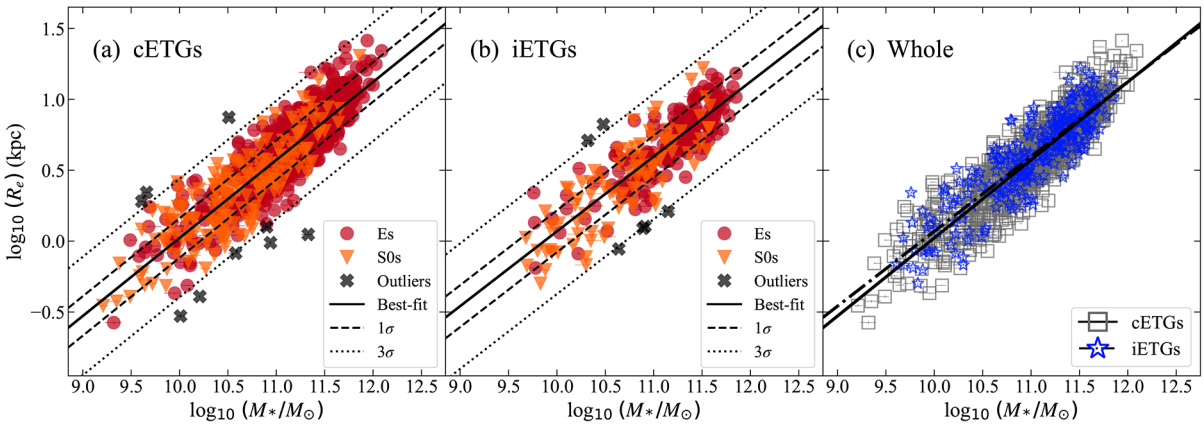

Fig. 5 The Mass-Size relation for (a) cETGs, (b) iETGs and (c) the whole sample (see key)

Table 7 MSR coefficients for our ETG samples obtained using LTS fitting technique. Slopes (column 2), zero-points (column 3), intrinsic scatters (column 4) and 1σ deviation (column 5) are displayed for both ETG samples

Sample	Fitting coefficients			
	$(\nu \pm \Delta\nu)$	$(\tau \pm \Delta\tau)$	$(\varepsilon \pm \Delta\varepsilon)$	1σ
cETGs	0.5501 ± 0.0086	-5.479 ± 0.096	0.1356 ± 0.0034	0.14
iETGs	0.528 ± 0.017	-5.21 ± 0.19	0.1446 ± 0.0067	0.15

and the stellar mass of the galaxy (M_*). This relation can be expressed as $R_e \propto M_*^{\nu}$, or in a logarithmic scale as

$$\log(R_e) = \nu \ \log(M_*) + \tau \tag{12}$$

In Fig. 5, we display the Mass-Size relation (Eq. (12)) for cETGs and iETGs in panels (a) and (b), respectively. Panel (c) represents the distribution of both samples as a function of environment. We excluded 9 cETG and 6 iETG outliers using the LTS-fitting technique. The best-fitting coefficients as well as the intrinsic scatter coefficient around the best-fit line are shown in Table 7. The coefficients of both samples are similar, with a slope (ν) equals 0.5501 ± 0.0086 for cETGs, and 0.528 ± 0.017 for iETGs. The slope of iETGs is within $3\sigma_{\rm comp}$ of that for cETGs. The zero-point (τ) for cETGs is -5.479 ± 0.096, whereas it is -5.21 ± 0.19 for iETGs. Also, the zero-point of iETGs is within $3\sigma_{\rm comp}$ of that for cETGs. In addition, the intrinsic scatter around the linear relations of cETGs and iETGs is nearly similar. We compare the slopes of our samples with those obtained by Chen et al. (2024) for quiescent galaxies in clusters and in the field at redshift $z < 0.1$. Their slopes ($\nu = 0.31$ for cluster quiescent galaxies and $\nu = 0.37$ for field quiescent galaxies) are smaller by about 28σ and 9σ than that for our cETG and iETG samples, respectively.

In Fig. 5, one sees that a large fraction of Es (circles) in both environments shows a tendency to be more massive and larger in size, compared to S0s (triangles) that appear distributed over a wider range of masses and sizes. The fraction of massive Es (with $\log(M_*/M_\odot) \geqslant 11$) in cETGs and iETGs are about 76% and 68%, respectively. This fraction is much smaller for S0s ($\sim 24\%$ for cETGs and $\sim 29\%$ for iETGs). Furthermore, galaxies with stellar masses ($\log(M_*/M_\odot) < 10.5$) are more scattered around the linear relation than the massive galaxies. A considerable fraction of these galaxies are S0s ($\sim 45\%$ in cETGs and $\sim 35\%$ in iETGs) and are generally younger than the massive ones.

In panel (c), over the entire range of stellar masses of both samples, iETGs exhibit a similar distribution to cETGs. At the massive end, both samples have nearly equal sizes for a specific fixed stellar mass. For example, massive ETGs whose stellar masses are $\log(M_*/M_\odot) = 11.5$ have R_e of 7.033 kpc for cETGs and 7.278 kpc for iETGs. Therefore, massive iETGs are about 3.5% larger than cETGs of the same stellar mass. At the low-mass end, the values of R_e that correspond to, for example, $\log(M_*/M_\odot = 10.0$ are 1.052 kpc and 1.175 kpc for cETGs and iETGs, respectively. This means that low-mass iETGs are about 11.5% larger than their cluster counterparts. Although the size-ratio of isolated-to-cluster ETGs decreases slightly with increasing the galactic stellar masses, the observed mass-size relation for both environments remains roughly the same. This means that nearby ETGs in clusters and in the field in our samples have similar trends, which in turn implies that a little statistically detected impact of the environment on the observed properties of ETGs.

A plausible explanation for this observed similarity is that massive ETGs in both environments may have formed at early epochs, quickly transformed their gas content into stars, and evolved passively by stellar aging and/or mergers (specially dry mergers) and interactions, supported by

what we find from the FP analysis for cETGs and iETGs. Massive ETGs in clusters and the field have generally older stellar population than low-mass ETGs. In contrast to massive ETGs, low-mass cluster and isolated ETGs have to be explained separately.

Low-mass cETGs may have suffered from processes such as tidal stripping due to the gravitational interactions with the surrounding galaxies and/or ram pressure stripping by the hot halo that removes the gas content and suppresses any further star formation. On the other hand, low-mass iETGs may have experienced wet merging or interactions with other galaxies, resulting in recent star formation in the remnants. However, a spectral analysis is needed to confirm this explanation and to investigate the star formation histories.

Thomas et al. (2010) studied the environmental effect on a sample of ETGs from SDSS DR4 within redshift range ($0.05 \leq z \leq 0.06$). The results showed that the effect of environment begins to increase with decreasing the stellar mass of the galaxy, consistent with this work. Bernardi et al. (2011) suggested that galaxies with stellar masses larger than $2 \times 10^{11} M_{\odot}$ have likely grown in sizes by major dry mergers that leave the velocity dispersion of the merger remnant unaffected while galaxies with stellar masses below $3 \times 10^{10} M_{\odot}$ are likely evolving via wet merging. Similarly, Huertas-Company et al. (2013,b) found that the MSR depends on both the galactic morphology and the stellar mass range. Their results showed that Es dominate masses with $\log(M_*/M_{\odot}) \sim 11$ while S0 galaxies are the majority at lower stellar masses in the range ($10.5 < \log(M_*/M_{\odot}) < 11$), with no clear difference in the evolution of the galaxy size in both environments, which is in contradiction with this work. However, the authors did not discuss which of the merger route or mass-loss via quasar and/or stellar wind is the plausible scenario for this size-growth with stellar mass in both environments. Cebrián and Trujillo (2014) found that isolated low-mass ETGs are $\sim 3.5\%$ larger than their counterparts in clusters. This suggests that galaxies in clusters could be formed earlier than those in the field and that they originate from a more homogeneous set of progenitors because of their less scattering than the isolated galaxies. This agrees with our findings except that low-mass iETGs in this study are about 11.5% larger than cETGs.

We found that massive galaxies are larger with a little statistically-detected dependence on their environments which is in agreement with Lacerna et al. (2016). However, Yoon et al. (2017) found that nearby massive galaxies ($M \geq 10^{11.2} M_{\odot}$) are about $20\% - 40\%$ larger in dense environments than their counterparts in less dense regions, which contradicts with our results. Yoon et al. (2017) concluded that these nearby massive galaxies have hierarchically grown in their sizes through frequent mergers with other galaxies.

More recently, Yoon et al. (2023) found differences in mass-size relation in that Low-mass Quiescent Galaxies (LQGs) in high-density environments exhibit a shallower slope compared to those in isolated environments. The authors concluded that recent gas-rich mergers affect the transformation from star-forming to quiescent galaxies since LQGs in dense environments have more disk-like structures, compared to those in low-density environments. This finding is in contrast with our results. However, Yoon et al. (2023) found that High-mass Quiescent Galaxies (HQGs) show a nearly identical mass-size relation across all environments, consistent with our results. Finally, Chen et al. (2024) showed a slight difference in the mass-size relation observed between cluster galaxies (other than BCGs) and the isolated ones, inline with our results.

5 Conclusions and summary

The current study investigated the role of environment in shaping the structural and kinematic properties of nearby ETGs. The studied samples were extracted from the latest release of Mapping Nearby Galaxies at APO (MaNGA) survey which is part of the SDSS-IV DR17 (Abdurro'uf et al. 2022). The morphological classification of the ETG sample (Es and S0s) was selected from *MaNGA Deep Learning Morphology DR17 Value-Added Catalog* (MDLM-VAC; Domínguez Sánchez et al. 2022) while the characterization of their host environments was taken from *Galaxy Environment for MaNGA Value-Added Catalog* (GEMA-VAC). The studied sample contains 946 ETGs in clusters (cETGs) and 288 isolated ETGs (iETGs) within a spectroscopic redshift ($z_{\rm spec} \leq 0.15$). We utilized CasJobs tool to extract the observable parameters of the selected samples (see Table 2). The physical parameters (e.g. R_e, $\langle \mu_e \rangle$, M_r and σ_0) were calculated to study the different scaling relations: the Fundamental Plane (FP), the Kormendy relation (KR), the Faber-Jackson relation (FJR) and the Mass-Size relation (MSR). The results of all scaling relations show a little dependence of the studied ETGs on their host environments. In addition, the results revealed that Es are, generally, less-scattered than S0s. The main conclusions of this study can be summarized as follows.

1. **The FP relation:**

- For cETGs, the FP is on the form ($\log R_e = 1.272 \log \sigma_0 + 0.3304 \langle \mu_e \rangle - 8.884$) whereas for iETGs it is expressed as ($\log R_e = 1.145 \log \sigma_0 + 0.2871 \langle \mu_e \rangle - 7.71$) which means that a considerable fraction of large cETGs ($\approx 49\%$) and iETGs ($\approx 38\%$) have σ_0 higher than 225 km/sec as well as higher values of $\langle \mu_e \rangle$ (i.e. lower surface brightnesses).
- The coefficients (a, b and c) for iETGs are within $7\sigma_{\rm comp}$, $12\sigma_{\rm comp}$ and $15\sigma_{\rm comp}$ of those for cETGs. The smaller

zero-point (c) for cETGs implies that cETGs have larger mass-to-light ratios, compared to iETGs.
- The analysis of the residuals showed that most S0s are more scattered around the FP than Es in both environments. This can be attributed to variations in the age and/or metallicity trends of the stellar population.

2. **The KR:**

- There are little statistically detected environmental effects on galaxies; cETGs and iETGs show similarities in their distributions. The obtained KR is ($\langle\mu_e\rangle = 1.886\log(R_e) + 18.672$) for cETGs while it is ($\langle\mu_e\rangle = 2.030\log(R_e) + 18.604$) for iETGs. The slope ($\alpha$) and zero-point ($\beta$) for iETGs are within $4\sigma_{\rm comp}$ and $3\sigma_{\rm comp}$ of that for cETGs, respectively.
- Large ETGs have higher $\langle\mu_e\rangle$ values and hence slightly less luminous than smaller ones.
- In both environments, the distribution of Es is concentrated toward larger sizes while S0s are widely distributed over the entire range of sizes.

3. **The FJR:**

- The FJRs for cETGs and iETGs are $L_r \propto \sigma_0^{2.752}$ and $L_r \propto \sigma_0^{2.451}$, respectively. The slope (η) and the zero-point (γ) of iETGs are both within $6\sigma_{\rm comp}$ of that for cETGs.
- The analysis showed that cETGs with ($\log(\sigma_0) \geq 2.35$) are $\sim 5\%$ less luminous than iETGs while cETGs with ($\log(\sigma_0) \leq 2.0$) are $\sim 25\%$ less luminous than iETGs.
- A large fraction of Es are concentrated at higher σ_0 (about 57% of cluster Es and 51% of isolated Es have $\log\sigma_0 \geq 2.35$) while S0s are more scattered around the FJR fitted line, in particular, towards the lower-luminosity part.

4. **The MSR:**

- In general, both cETGs and iETGs have sizes that are directly proportional to their stellar mass content.
- The slope (ν) equals 0.5501 ± 0.0086 for cETGs and 0.528 ± 0.017 for iETGs while the zero-point (τ) for cETGs is -5.479 ± 0.096 whereas it is -5.21 ± 0.19 for iETGs. These iETGs coefficients are both within $3\sigma_{\rm comp}$ of those for cETGs.
- Massive iETGs ($\log(M_*/M_\odot) = 11.5$) are about 3.5% larger than cETGs whereas low-mass cETGs ($\log(M_*/M_\odot) = 10.0$) have sizes $\sim 11.5\%$ smaller than iETGs of the same stellar mass.
- The majority of massive ETGs are Es while low-mass ETGs are generally S0s in both samples.

5. Massive galaxies may have formed their stars at early epochs and evolved passively since their formation, by stellar aging (Saracco et al. 2014) and/or dry mergers (Trussler et al. 2021; Yoon and Park 2022). As a result, the observed remnants would have larger sizes and stellar masses without affecting other properties.
6. Low-mass cETGs may have experienced environmental mechanisms that cease any further star formation (e.g. ram-pressure stripping and/or tidal interactions), leaving the remnant with lower stellar mass and luminosity.
7. Furthermore, low-mass iETGs may have undergone a recent gaseous merger. This would induce a new star formation episode in the remnant and result in the observed smaller mass-to-light ratios for iETGs than their cluster counterparts.

However, we may need to conduct a further spectral analysis for the stellar populations. Also, larger galaxy samples in different densities and redshifts are needed to be able to study their formation and evolution routes.

Acknowledgements The authors are grateful to Dr. Reham El-Kholy (Astronomy, Space Science and Meteorology Department, Faculty of Science, Cairo University, Giza, Egypt) for her help in resolving some issues in the python code. EA is thankful to Dr. Mohamed H. Abdullah (Department of Astronomy, National Research Institute of Astronomy and Geophysics, Helwan, Egypt) for explaining important statistical aspects and fruitful discussion. Funding for the Sloan Digital Sky Survey IV has been provided by the Alfred P. Sloan Foundation, the U.S. Department of Energy Office of Science, and the Participating Institutions. SDSS acknowledges support and resources from the Center for High-Performance Computing at the University of Utah. The SDSS web site is www.sdss4.org. SDSS is managed by the Astrophysical Research Consortium for the Participating Institutions of the SDSS Collaboration including the Brazilian Participation Group, the Carnegie Institution for Science, Carnegie Mellon University, Center for Astrophysics | Harvard & Smithsonian (CfA), the Chilean Participation Group, the French Participation Group, Instituto de Astrofísica de Canarias, The Johns Hopkins University, Kavli Institute for the Physics and Mathematics of the Universe (IPMU) / University of Tokyo, the Korean Participation Group, Lawrence Berkeley National Laboratory, Leibniz Institut für Astrophysik Potsdam (AIP), Max-Planck-Institut für Astronomie (MPIA Heidelberg), Max-Planck-Institut für Astrophysik (MPA Garching), Max-Planck-Institut für Extraterrestrische Physik (MPE), National Astronomical Observatories of China, New Mexico State University, New York University, University of Notre Dame, Observatório Nacional / MCTI, The Ohio State University, Pennsylvania State University, Shanghai Astronomical Observatory, United Kingdom Participation Group, Universidad Nacional Autónoma de México, University of Arizona, University of Colorado Boulder, University of Oxford, University of Portsmouth, University of Utah, University of Virginia, University of Washington, University of Wisconsin, Vanderbilt University, and Yale University.

Author contributions E.A. and R.S. collected the data sample and with the help of Z.A, they analyzed the data and prepared the figures. E.A. and Z.A. wrote the main manuscript text. All authors reviewed the manuscript.

Data Availability No datasets were generated or analysed during the current study.

Declarations

Competing interests The authors declare no competing interests.

References

Abdurro'uf, Accetta, K., Aerts, C., et al.: The seventeenth data release of the sloan digital sky surveys: complete release of MaNGA, MaStar, and APOGEE-2 data. Astrophys. J. Suppl. Ser. **59**(2), 35 (2022). https://doi.org/10.3847/1538-4365/ac4414. arXiv:2112.02026 [astro-ph.GA]

Aceves, H., Velázquez, H.: From the Tully-Fisher relation to the fundamental plane through mergers. Mon. Not. R. Astron. Soc. **60**(1), L50–L54 (2005). https://doi.org/10.1111/j.1745-3933.2005.00044.x. arXiv:astro-ph/0412307 [astro-ph]

Argudo-Fernández, M., Verley, S., Bergond, G., et al.: Catalogues of isolated galaxies, isolated pairs, and isolated triplets in the local Universe. A&A **78**, A110 (2015). https://doi.org/10.1051/0004-6361/201526016. arXiv:1504.00117 [astro-ph.GA]

Argudo-Fernandez, M., Goddard, D., Thomas, D., et al.: Galaxy Environment for MaNGA Value-Added Catalog (2021). https://data.sdss.org/datamodel/files/MANGA_GEMA/GEMA_VER/GEMA.html [Online; accessed 8-June-2021]

Beck, R., Dobos, L., Budavári, T., et al.: Photometric redshifts for the SDSS data release 12. Mon. Not. R. Astron. Soc. **60**(2), 1371–1381 (2016). https://doi.org/10.1093/mnras/stw1009. arXiv:1603.09708 [astro-ph.GA]

Bekki, K.: The fundamental plane and merger scenario. I. Star formation history of galaxy mergers and origin of the fundamental plane. Astrophys. J. **96**(2), 713–727 (1998). https://doi.org/10.1086/305411. arXiv:astro-ph/9804069 [astro-ph]

Bernardi, M., Renzini, A., da Costa, L.N., et al.: Cluster versus field elliptical galaxies and clues on their formation. Astrophys. J. Lett. **08**(2), L143–L146 (1998). https://doi.org/10.1086/311742. arXiv:astro-ph/9810066 [astro-ph]

Bernardi, M., Sheth, R.K., Annis, J., et al.: Early-type galaxies in the sloan digital sky survey. II. Correlations between observables. Astron. J. **25**(4), 1849–1865 (2003). https://doi.org/10.1086/374256. arXiv:astro-ph/0301624 [astro-ph]

Bernardi, M., Sheth, R.K., Annis, J., et al.: Early-type galaxies in the sloan digital sky survey. III. The fundamental plane. Astron. J. **25**(4), 1866–1881 (2003b). https://doi.org/10.1086/367794. arXiv:astro-ph/0301626 [astro-ph]

Bernardi, M., Sheth, R.K., Nichol, R.C., et al.: A search for the most massive galaxies: double trouble? Astron. J. **31**(4), 2018–2034 (2006). https://doi.org/10.1086/499770. arXiv:astro-ph/0510696 [astro-ph]

Bernardi, M., Hyde, J.B., Fritz, A., et al.: A search for the most massive galaxies - II. Structure, environment and formation. Mon. Not. R. Astron. Soc. **91**(3), 1191–1209 (2008). https://doi.org/10.1111/j.1365-2966.2008.13876.x. arXiv:0809.2602 [astro-ph]

Bernardi, M., Roche, N., Shankar, F., et al.: Evidence of major dry mergers at $M_* > 2 \times 10^{11}$ $M_\odot$ from curvature in early-type galaxy scaling relations? Mon. Not. R. Astron. Soc. **12**(1), L6–L10 (2011). https://doi.org/10.1111/j.1745-3933.2010.00982.x. arXiv:1011.1501 [astro-ph.CO]

Bernardi, M., Domínguez Sánchez, H., Margalef-Bentabol, B., et al.: The stellar mass fundamental plane: the virial relation and a very thin plane for slow rotators. Mon. Not. R. Astron. Soc. **94**(4), 5148–5160 (2020). https://doi.org/10.1093/mnras/staa1064. arXiv:2004.07847 [astro-ph.GA]

Bolton, A.S., Schlegel, D.J., Aubourg, É., et al.: Spectral classification and redshift measurement for the SDSS-III baryon oscillation spectroscopic survey. Astron. J. **44**(5), 144 (2012). https://doi.org/10.1088/0004-6256/144/5/144. arXiv:1207.7326 [astro-ph.CO]

Boselli, A., Fossati, M., Sun, M.: Ram pressure stripping in high-density environments. Astron. Astrophys. Rev. **0**(1), 3 (2022). https://doi.org/10.1007/s00159-022-00140-3. arXiv:2109.13614 [astro-ph.GA]

Bundy, K., Bershady, M.A., Law, D.R., et al.: Overview of the SDSS-IV MaNGA survey: mapping nearby galaxies at apache point observatory. Astrophys. J. **98**(1), 7 (2015). https://doi.org/10.1088/0004-637X/798/1/7. arXiv:1412.1482 [astro-ph.GA]

Calvi, R., Poggianti, B.M., Fasano, G., et al.: The distribution of galaxy morphological types and the morphology-mass relation in different environments at low redshift. Mon. Not. R. Astron. Soc. **19**(1), L14–L18 (2012). https://doi.org/10.1111/j.1745-3933.2011.01168.x10.1086/122140. arXiv:1110.0802 [astro-ph.CO]

Capelato, H.V., de Carvalho, R.R., Carlberg, R.G.: Mergers of dissipationless systems: clues about the fundamental plane. Astrophys. J. **51**, 525 (1995). https://doi.org/10.1086/176240

Cappellari, M., Bacon, R., Bureau, M., et al.: The SAURON project - IV. The mass-to-light ratio, the virial mass estimator and the fundamental plane of elliptical and lenticular galaxies. Mon. Not. R. Astron. Soc. **66**(4), 1126–1150 (2006). https://doi.org/10.1111/j.1365-2966.2005.09981.x. arXiv:astro-ph/0505042 [astro-ph]

Cappellari, M., Scott, N., Alatalo, K., et al.: The ATLAS^{3D} project - XV. Benchmark for early-type galaxies scaling relations from 260 dynamical models: mass-to-light ratio, dark matter, fundamental plane and mass plane. Mon. Not. R. Astron. Soc. **32**(3), 1709–1741 (2013). https://doi.org/10.1093/mnras/stt562. arXiv:1208.3522 [astro-ph.CO]

Cebrián, M., Trujillo, I.: The effect of the environment on the stellar mass-size relationship for present-day galaxies. Mon. Not. R. Astron. Soc. **44**(1), 682–699 (2014). https://doi.org/10.1093/mnras/stu1375. arXiv:1404.7135 [astro-ph.GA]

Chen, Z., Gu, Y., Zou, H., et al.: Galaxy clusters from the DESI legacy imaging surveys. II. Environmental effects on the size–mass relation. Astrophys. J. **61**(2), 253 (2024). https://doi.org/10.3847/1538-4357/ad15fd. arXiv:2312.17075 [astro-ph.GA]

Cherinka, B., Andrews, B.H., Sánchez-Gallego, J., et al.: Marvin: a tool kit for streamlined access and visualization of the SDSS-IV MaNGA data set. Astron. J. **58**(2), 74 (2019). https://doi.org/10.3847/1538-3881/ab2634. arXiv:1812.03833 [astro-ph.IM]

Cimatti, A., Fraternali, F., Nipoti, C.: Introduction to Galaxy Formation and Evolution: From Primordial Gas to Present-Day Galaxies. Cambridge University Press, Cambridge (2020)

Ciotti, L., Lanzoni, B., Renzini, A.: The tilt of the fundamental plane of elliptical galaxies - I. Exploring dynamical and structural effects. Mon. Not. R. Astron. Soc. **82**(1), 1–12 (1996). https://doi.org/10.1093/mnras/282.1.1. arXiv:astro-ph/9601100 [astro-ph]

de Carvalho, R.R., Djorgovski, S.: Systematic differences between the field and cluster elliptical galaxies. Astrophys. J. Lett. **89**, L49 (1992). https://doi.org/10.1086/186346

de Graaff, A., Bezanson, R., Franx, M., et al.: The fundamental plane in the LEGA-C survey: unraveling the M/L ratio variations of massive star-forming and quiescent galaxies at z $\sim$ 0.8. Astrophys. J. **13**(2), 103 (2021). https://doi.org/10.3847/1538-4357/abf1e7. arXiv:2103.12753 [astro-ph.GA]

de Vaucouleurs, G.: Recherches sur les nebuleuses extragalactiques. Ann. Astrophys. **11**, 247 (1948)

Deng, X.F., He, J.Z., Wu, P.: Effects of both extremes of environments on galaxy properties. A&A **84**(2), 355–360 (2008). https://doi.org/10.1051/0004-6361:20078849

Djorgovski, S., Davis, M.: Fundamental properties of elliptical galaxies. Astrophys. J. **13**, 59 (1987). https://doi.org/10.1086/164948

Domínguez Sánchez, H., Bernardi, M., Nikakhtar, F., et al.: Galaxy properties as revealed by MaNGA - III. Kinematic profiles and stellar population gradients in S0s. Mon. Not. R. Astron. Soc. **95**(3), 2894–2908 (2020). https://doi.org/10.1093/mnras/staa1364. arXiv:2005.07693 [astro-ph.GA]

Domínguez Sánchez, H., Margalef, B., Bernardi, M., et al.: SDSS-IV DR17: final release of MaNGA PyMorph photometric and deep-learning morphological catalogues. Mon. Not. R. Astron. Soc. **09**(3), 4024–4036 (2022). https://doi.org/10.1093/mnras/stab3089. arXiv:2110.10694 [astro-ph.GA]

D'Onofrio, M., Chiosi, C.: The fundamental plane in the hierarchical context. A&A **61**, A150 (2022). https://doi.org/10.1051/0004-6361/202142851. arXiv:2112.03574 [astro-ph.GA]

D'Onofrio, M., Fasano, G., Varela, J., et al.: The fundamental plane of early-type galaxies in nearby clusters from the WINGS database. Astrophys. J. **85**(2), 875–896 (2008). https://doi.org/10.1086/591143. arXiv:0804.1892 [astro-ph]

Dressler, A.: Galaxy morphology in rich clusters: implications for the formation and evolution of galaxies. Astrophys. J. **36**, 351–365 (1980). https://doi.org/10.1086/157753

Dressler, A., Lynden-Bell, D., Burstein, D., et al.: Spectroscopy and photometry of elliptical galaxies. I. New distance estimator. Astrophys. J. **13**, 42 (1987). https://doi.org/10.1086/164947

Dressler, A., Oemler, A. Jr., Couch, W.J., et al.: Evolution since z = 0.5 of the morphology-density relation for clusters of galaxies. Astrophys. J. **90**(2), 577–591 (1997). https://doi.org/10.1086/304890. arXiv:astro-ph/9707232 [astro-ph]

Emsellem, E., Cappellari, M., Krajnović, D., et al.: The SAURON project - IX. A kinematic classification for early-type galaxies. Mon. Not. R. Astron. Soc. **79**(2), 401–417 (2007). https://doi.org/10.1111/j.1365-2966.2007.11752.x. arXiv:astro-ph/0703531 [astro-ph]

Evstigneeva, E.A., Reshetnikov, V.P., Sotnikova, N.Y.: Effect of the environment on the fundamental plane of elliptical galaxies. A&A **81**, 6–12 (2002). https://doi.org/10.1051/0004-6361:20011379. arXiv:astro-ph/0110105 [astro-ph]

Faber, S.M., Jackson, R.E.: Velocity dispersions and mass-to-light ratios for elliptical galaxies. Astrophys. J. **04**, 668–683 (1976). https://doi.org/10.1086/154215

Faber, S.M., Dressler, A., Davies, R.L., et al.: Global scaling relations for elliptical galaxies and implications for formation. In: Faber, S.M. (ed.) Nearly Normal Galaxies. From the Planck Time to the Present, p. 175 (1987)

Ferreras, I.: Fundamentals of Galaxy Dynamics, Formation and Evolution. UCL Press (2019)

Focardi, P., Malavasi, N.: The effect of the environment on the Faber-Jackson relation. Astrophys. J. **56**(2), 117 (2012). https://doi.org/10.1088/0004-637X/756/2/117. arXiv:1207.2750 [astro-ph.CO]

Forbes, D.A., Ponman, T.J., Brown, R.J.N.: Dependence of the fundamental plane scatter on galaxy age. Astrophys. J. Lett. **08**(1), L43–L46 (1998). https://doi.org/10.1086/311715. arXiv:astro-ph/9809319 [astro-ph]

Gu, Y., Fang, G., Yuan, Q., et al.: The effect of environment on star formation activity and morphology at 0.5 < z < 2.5 in CANDELS. Astrophys. J. **21**(1), 60 (2021). https://doi.org/10.3847/1538-4357/ac1ce0. arXiv:2109.11261 [astro-ph.GA]

Hahn, O., Porciani, C., Carollo, C.M., et al.: Properties of dark matter haloes in clusters, filaments, sheets and voids. Mon. Not. R. Astron. Soc. **75**(2), 489–499 (2007). https://doi.org/10.1111/j.1365-2966.2006.11318.x. arXiv:astro-ph/0610280 [astro-ph]

Hamabe, M., Kormendy, J.: Correlations between R/1/4 - law parameters for bulges and elliptical galaxies. In: de Zeeuw, P.T. (ed.) Structure and Dynamics of Elliptical Galaxies, p. 379 (1987). https://doi.org/10.1007/978-94-009-3971-4_32

Hopkins, P.F., Cox, T.J., Hernquist, L.: Dissipation and the fundamental plane: observational tests. Astrophys. J. **89**(1), 17–48 (2008). https://doi.org/10.1086/592105. arXiv:0806.3974 [astro-ph]

Hou, L., Wang, Y.: The fundamental plane relation of early-type galaxies: environmental dependence. Res. Astron. Astrophys. **5**(5), 651–662 (2015). https://doi.org/10.1088/1674-4527/15/5/004

Huertas-Company, M., Mei, S., Shankar, F., et al.: The evolution of the mass-size relation for early-type galaxies from z ∼ 1 to the present: dependence on environment, mass range and detailed morphology. Mon. Not. R. Astron. Soc. **28**(2), 1715–1742 (2013). https://doi.org/10.1093/mnras/sts150. arXiv:1207.5793 [astro-ph.CO]

Huertas-Company, M., Shankar, F., Mei, S., et al.: No evidence for a dependence of the mass-size relation of early-type galaxies on environment in the local Universe. Astrophys. J. **79**(1), 29 (2013b). https://doi.org/10.1088/0004-637X/779/1/29. arXiv:1212.4143 [astro-ph.CO]

Hyde, J.B., Bernardi, M.: The luminosity and stellar mass fundamental plane of early-type galaxies. Mon. Not. R. Astron. Soc. **96**(2), 1171–1185 (2009). https://doi.org/10.1111/j.1365-2966.2009.14783.x. arXiv:0810.4924 [astro-ph]

Jorgensen, I., Franx, M., Kjaergaard, P.: Spectroscopy for E and S0 galaxies in nine clusters. Mon. Not. R. Astron. Soc. **76**(4), 1341–1364 (1995). https://doi.org/10.1093/mnras/276.4.1341

Karachentseva, V.E.: The catalogue of isolated galaxies. Astrofiz. Issled. Izv. Spets. Astrofiz. Obs. **8**, 3–49 (1973)

Kelvin, L.S., Driver, S.P., Robotham, A.S.G., et al.: Galaxy and Mass Assembly (GAMA): ugrizYJHK Sérsic luminosity functions and the cosmic spectral energy distribution by Hubble type. Mon. Not. R. Astron. Soc. **39**(2), 1245–1269 (2014). https://doi.org/10.1093/mnras/stt2391. arXiv:1401.1817 [astro-ph.CO]

Kormendy, J.: Brightness distributions in compact and normal galaxies. II. Structure parameters of the spheroidal component. Astrophys. J. **18**, 333–346 (1977). https://doi.org/10.1086/155687

Kroupa, P.: On the variation of the initial mass function. Mon. Not. R. Astron. Soc. **22**(2), 231–246 (2001). https://doi.org/10.1046/j.1365-8711.2001.04022.x. arXiv:astro-ph/0009005 [astro-ph]

La Barbera, F., Lopes, P.A.A., de Carvalho, R.R., et al.: SPIDER - III. Environmental dependence of the fundamental plane of early-type galaxies. Mon. Not. R. Astron. Soc. **08**(3), 1361–1386 (2010). https://doi.org/10.1111/j.1365-2966.2010.17273.x. arXiv:1003.1119 [astro-ph.CO]

La Barbera, F., Ferreras, I., de Carvalho, R.R., et al.: On the radial stellar content of early-type galaxies as a function of mass and environment. Astrophys. J. Lett. **40**(2), L41 (2011). https://doi.org/10.1088/2041-8205/740/2/L41. arXiv:1108.0946 [astro-ph.CO]

Lacerna, I., Hernández-Toledo, H.M., Avila-Reese, V., et al.: Isolated elliptical galaxies in the local Universe. A&A **88**, A79 (2016). https://doi.org/10.1051/0004-6361/201527844. arXiv:1511.08809 [astro-ph.GA]

Maraston, C., Strömbäck, G., Thomas, D., et al.: Modelling the colour evolution of luminous red galaxies - improvements with empirical stellar spectra. Mon. Not. R. Astron. Soc. **94**(1), L107–L111 (2009). https://doi.org/10.1111/j.1745-3933.2009.00621.x. arXiv:0809.1867 [astro-ph]

Nigoche-Netro, A., Moles, M., Ruelas-Mayorga, A., et al.: Structural properties of isolated early-type galaxies. The dependence of scaling relations on environment. A&A **72**(3), 773–784 (2007a). https://doi.org/10.1051/0004-6361:20066398

Nigoche-Netro, A., Moles, M., Ruelas-Mayorga, A., et al.: Structural properties of isolated early-type galaxies. The dependence of scaling relations on environment. A&A **72**(3), 773–784 (2007b). https://doi.org/10.1051/0004-6361:20066398

Nigoche-Netro, A., Aguerri, J.A.L., Lagos, P., et al.: The intrinsic dispersion in the Faber-Jackson relation for early-type galaxies as function of the mass and redshift. A&A **34**, A61 (2011). https://doi.org/10.1051/0004-6361/201016360. arXiv:1107.6017 [astro-ph.CO]

Pahre, M.A., Djorgovski, S.G., de Carvalho, R.R.: Near-infrared imaging of early-type galaxies. III. The near-infrared fundamental plane. Astron. J. **16**(4), 1591–1605 (1998). https://doi.org/10.1086/300544. arXiv:astro-ph/9806315 [astro-ph]

Postman, M., Geller, M.J.: The morphology-density relation - the group connection. Astrophys. J. **81**, 95–99 (1984). https://doi.org/10.1086/162078

Reda, F.M., Forbes, D.A., Hau, G.K.T.: The fundamental plane of isolated early-type galaxies. Mon. Not. R. Astron. Soc. **60**(2), 693–702 (2005). https://doi.org/10.1111/j.1365-2966.2005.09058.x. arXiv:astro-ph/0505265 [astro-ph]

Renzini, A.: Stellar population diagnostics of elliptical galaxy formation. Annu. Rev. Astron. Astrophys. **4**(1), 141–192 (2006). https://doi.org/10.1146/annurev.astro.44.051905.092450. arXiv:astro-ph/0603479 [astro-ph]

Rettura, A., Rosati, P., Nonino, M., et al.: Formation epochs, star formation histories, and sizes of massive early-type galaxies in cluster and field environments at z = 1.2: insights from the rest-frame ultraviolet. Astrophys. J. **09**(1), 512–524 (2010). https://doi.org/10.1088/0004-637X/709/1/512. arXiv:0806.4604 [astro-ph]

Robertson, B., Cox, T.J., Hernquist, L., et al.: The fundamental scaling relations of elliptical galaxies. Astrophys. J. **41**(1), 21–40 (2006). https://doi.org/10.1086/500360. arXiv:astro-ph/0511053 [astro-ph]

Samir, R.M., Reda, F.M., Shaker, A.A., et al.: The fundamental plane of early-type galaxies in different environments. NRIAG J. Astron. Geophys. **2**, 277–288 (2016). https://doi.org/10.1016/j.nrjag.2016.06.004

Samir, R.M., Takey, A., Shaker, A.A.: The fundamental plane of brightest cluster galaxies and isolated elliptical galaxies. Astrophys. Space Sci. **65**(8), 142 (2020). https://doi.org/10.1007/s10509-020-03857-8

Saracco, P., Casati, A., Gargiulo, A., et al.: Scaling relations of cluster elliptical galaxies at z ∼ 1.3. Distinguishing luminosity and structural evolution. A&A **67**, A94 (2014). https://doi.org/10.1051/0004-6361/201423495. arXiv:1401.5600 [astro-ph.GA]

Schechter, P.: An analytic expression for the luminosity function for galaxies. Astrophys. J. **03**, 297–306 (1976). https://doi.org/10.1086/154079

Taranu, D., Dubinski, J., Yee, H.K.C.: Mergers in galaxy groups. II. The fundamental plane of elliptical galaxies. Astrophys. J. **03**(2), 78 (2015). https://doi.org/10.1088/0004-637X/803/2/78. arXiv:1406.2693 [astro-ph.GA]

Taylor, M.B.: TOPCAT & STIL: starlink table/VOTable processing software. In: Shopbell, P., Britton, M., Ebert, R. (eds.) Astronomical Data Analysis Software and Systems XIV, p. 29 (2005)

Thomas, D., Maraston, C., Schawinski, K., et al.: Environment and self-regulation in galaxy formation. Mon. Not. R. Astron. Soc. **04**(4), 1775–1789 (2010). https://doi.org/10.1111/j.1365-2966.2010.16427.x. arXiv:0912.0259 [astro-ph.CO]

Trevisan, M., Ferreras, I., de La Rosa, I.G., et al.: Constraints on feedback processes during the formation of early-type galaxies. Astrophys. J. Lett. **52**(2), L27 (2012). https://doi.org/10.1088/2041-8205/752/2/L27. arXiv:1203.4775 [astro-ph.CO]

Trussler, J., Maiolino, R., Maraston, C., et al.: The weak imprint of environment on the stellar populations of galaxies. Mon. Not. R. Astron. Soc. **00**(4), 4469–4490 (2021). https://doi.org/10.1093/mnras/staa3545. arXiv:2006.01154 [astro-ph.GA]

Wang, H., Mo, H.J., Yang, X., et al.: ELUCID - exploring the local Universe with ReConstructed initial density field III: constrained simulation in the SDSS volume. Astrophys. J. **31**(2), 164 (2016). https://doi.org/10.3847/0004-637X/831/2/164. arXiv:1608.01763 [astro-ph.CO]

Wegner, G., Colless, M., Saglia, R.P., et al.: The peculiar motions of early-type galaxies in two distant regions - II. The spectroscopic data. Mon. Not. R. Astron. Soc. **05**(2), 259–296 (1999). https://doi.org/10.1046/j.1365-8711.1999.02339.x. arXiv:astro-ph/9811241 [astro-ph]

Westfall, K.B., Cappellari, M., Bershady, M.A., et al.: The data analysis pipeline for the SDSS-IV MaNGA IFU galaxy survey: overview. Astron. J. **58**(6), 231 (2019). https://doi.org/10.3847/1538-3881/ab44a2. arXiv:1901.00856 [astro-ph.GA]

Wright, E.L.: A cosmology calculator for the World Wide Web. Publ. Astron. Soc. Pac. **18**(850), 1711–1715 (2006). https://doi.org/10.1086/510102. arXiv:astro-ph/0609593 [astro-ph]

Yoon, Y., Park, C.: Dependence of the fundamental plane of early-type galaxies on age and internal structure. Astrophys. J. **97**(2), 121 (2020). https://doi.org/10.3847/1538-4357/ab9b26. arXiv:2006.12141 [astro-ph.GA]

Yoon, Y., Park, C.: The fundamental plane is not a plane: warped nature of the fundamental plane of early-type galaxies and its implication for galaxy formation. Astrophys. J. **36**(1), 22 (2022). https://doi.org/10.3847/1538-4357/ac854a. arXiv:2208.07656 [astro-ph.GA]

Yoon, Y., Im, M., Kim, J.W.: Massive galaxies are larger in dense environments: environmental dependence of mass-size relation of early-type galaxies. Astrophys. J. **34**(1), 73 (2017). https://doi.org/10.3847/1538-4357/834/1/73. arXiv:1612.07945 [astro-ph.GA]

Yoon, Y., Ko, J., Kim, J.W.: Impact of galaxy mergers on stellar population profiles of early-type galaxies. Astrophys. J. **46**(1), 41 (2023). https://doi.org/10.3847/1538-4357/acbcc5. arXiv:2303.00559 [astro-ph.GA]